Indian Journal of Engineering & Materials Sciences
Vol. 15, October 2008, pp. 382-390

Micromechanical analysis of FRP hybrid composite lamina for in-plane transverse loading

K Sivaji Babu[a]*, K Mohana Rao[b], V Rama Chandra Raju[c], V Bala Krishna Murthy[d] & M S R Niranjan Kumar[e]

[a]Department of Mechanical Engineering, V R Siddhartha Engineering College, Vijayawada 520 007, India

[b]C R Reddy Engineering College, Eluru 534 007, India

[c]J N T University, Vizayanagaram 535 002, India

[d]Department of Mechanical Engineering, P.V.P. Siddhartha Institute of Technology, Vijayawada 520 007, India

[e]Department of Production Engineering, V.R. Siddhartha Engineering College, Vijayawada 520 007, India

Received 9 September 2007; accepted 19 June 2008

In this paper, the micromechanical behaviour of the square unit cell of a hybrid fiber reinforced composite lamina consisting of graphite and boron fibers embedded in epoxy matrix, has been studied. A three-dimensional finite element model with governing boundary conditions has been developed from the unit cells of square pattern of the composite to predict the Young's modulus (E_2) and Poisson's ratios (ν_{21} and ν_{23}) of graphite-boron hybrid fiber reinforced lamina for various volume fractions. The stresses at the fiber-matrix interfaces induced due to the in-plane transverse loading, that is applied to predict the in-plane transverse Young's modulus (E_2) and the associated Poisson's ratios, are also determined from these models. The finite element software ANSYS has been successfully executed to evaluate the properties and stresses. The variation of the stresses at the fiber-matrix interface with respect to the angular location is discussed. The Young's modulus is found to be increasing with V_f indicating that the stiffness of the composite increases with V_f , The magnitude of the normal stresses at the fiber matrix interface are maximum at $\theta = 0°$ as the direction of the load is normal to the surface at this location. This may result in the separation of fiber and matrix leading to debonding. This analysis is useful to realize the advantages of hybrid fiber-reinforced composites in structural applications, and to identify the locations with reasons where the stresses are critical to damage the interface.

Keywords: FEM, Hybrid FRP, Interface, Micromechanics

Fiber reinforced composites can be tailor made, as their properties can be controlled by the appropriate selection of the substrata parameters such as fiber orientation, volume fraction, fiber spacing, and layer sequence. The required directional properties can be achieved in the case of fiber reinforced composites by properly selecting various parameters enlisted above. As a result of this, the designer can have a tailor-made material with the desired properties. Such a material design reduces the weight and improves the performance of the composite. For example, the carbon-carbon composites are strong in the direction of the fiber reinforcement but weak in the other directions. Elastic constants of fiber reinforced composites with various types of constituents were determined by Chen and Chang[1], Hashin and Rosen[2], Hashin[3] and Whitney[4].

It is clear from the above predictions, i.e., elastic constants of fiber-reinforced composites, that four of the five independent composite constants (E_1, E_2, ν_{12}, G_{12} and G_{23}) differ only in their expressions for the fifth elastic constant, i.e., transverse shear modulus, which varies between two bounds that are reasonably close for the cases of practical interest. The values of elastic Moduli presented by Hashin and Rosen[2] have very close bounds. Ishikawa *et al.*[5] experimentally obtained all the independent elastic Moduli of unidirectional carbon-epoxy composites with the tensile and torsional tests of co-axis and off-axis specimens. They confirmed the transverse isotropy nature of the graphite-epoxy composites. Hashin[6] comprehensively reviewed the analysis of composite materials with respect to mechanical and materials point of view. Expressions for E_1 and G_{12} are derived using the theory of elasticity approach[7].

Micromechanics

Micromechanics is intended to study the distribution of stresses and strains within the micro regions of the composite under loading. This study will be particularized to simple loading and geometry for evaluating the average or composite stiffnesses

*For correspondence (E-mail: k_sivajibabu@rediffmail.com)

and strengths of the composites[7,8]. Micromechanics analysis can be carried theoretically using the principles of continuum mechanics, and experimentally using mechanical, photo elasticity, ultrasonic tests, etc. The results of micromechanics will help to (i) understand load sharing among the constituents of the composites, microscopic structure (arrangement of fibers), etc., within composites, (ii) understand the influence of microstructure on the properties of composite, (iii) predict the average properties of the lamina, and (iv) design the materials, i.e., constituents volume fractions, their distribution and orientation, for a given situation.

The properties and behaviour of a composite are influenced by the properties of fiber and matrix, interfacial bond and by its microstructure. Microstructural parameters that influence the composite behaviour are fiber diameter, length, volume fraction, packing and orientation of fiber. A closed form micromechanical equation for predicting the transverse modulus (E_2) of continuous fiber reinforced polymers is presented[9].

Anifantis[10] predicted the micromechanical stress state developed within fibrous composites that contain a heterogeneous inter phase region by applying finite element method to square and hexagonal arrays of fibers. Sun *et al.*[11] established a vigorous mechanics foundation for using a representative volume element (RVE) to predict the mechanical properties of unidirectional fiber composites. Li[12] has developed two typical idealized packing systems, which have been employed for unidirectional fiber reinforced composites, viz., square and hexagonal ones to accommodate fibers of irregular cross sections and imperfections asymmetrically distributed around fibers. To understand the mechanism of the 'hybrid effect' on the tensile properties of hybrid composites Qiu and Schwartz[13] investigated the fiber/matrix interface properties by using single fiber pull out from a micro composite (SFPOM) test, which showed a significant difference between the interfacial shear strength of Kevlar fiber/epoxy in single fiber type and that in the hybrid at a constant fiber volume fraction, which shortened the ineffective length and contributed to the failure strain increase of Kevlar fibers in the hybrid. Mishra and Mohanthy *et al.*[14] investigated the degree of mechanical reinforcement that could be obtained by the introduction of glass fibers in bio fiber (pineapple leaf fiber/sisal fiber) reinforced polyester composite experimentally. Addition of relatively small amount of glass fiber to the pineapple leaf fiber and sisal fiber reinforced polyester matrix enhanced the mechanical properties of the resulting hybrid composites. The works reported in the available literature do not include the micromechanical analysis of hybrid FRP lamina using FEM. The present work aims do develop a 3-D finite element model for the micromechanical analysis of hybrid composite lamina.

Square array of unit cells

A schematic diagram of the unidirectional fiber composite is shown in Fig. 1 where the fibers are arranged in the square array. It is assumed that the fiber and matrix materials are linearly elastic. A unit cell is adopted for the analysis. The cross sectional area of the fiber relative to the total cross sectional area of the unit cell is a measure of the volume of fiber relative to the total volume of the composite. This fraction is an important parameter in composite materials and is called fiber volume fraction (V_f).

Problem statement

The analysis deals with the evaluation of the in-plane transverse Young's modulus E_2, Poison's ratios ν_{21}, ν_{23} and determination of the stresses at the fiber-matrix interfaces for a complete possible range of fiber volume fractions using 3-D finite element analysis based on theory of elasticity.

Finite element model

The 1-2-3 coordinate system shown in Fig. 2 is used to study the behavior of unit cell. The isolated

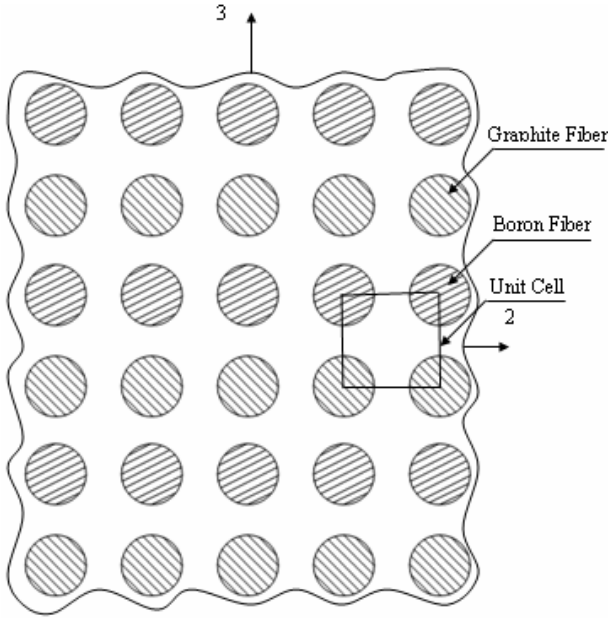

Fig. 1 — Concept of unit cells

unit cell behaves as a part of large array of unit cells by satisfying the conditions that the boundaries of the isolated unit cell remain plane.

It is assumed that the geometry, material and loading of unit cell are symmetric with respect to 1-2-3 coordinate system. Therefore, a one-fourth portion of the unit cell is modeled for the analysis (Fig. 3).

The dimensions of the finite element model are taken as (i) X=100 units (in-plane Transverse direction), (ii) Y=200 units (out-of-plane transverse direction) and (iii) Z=10 units (fiber direction).

The radius of fiber is varied corresponding to the volume fraction. For example, the radius of the fiber is calculated as 61.8 units, so that the fiber volume fraction becomes 0.30.

The element used for the present analysis is SOLID 95 of ANSYS software[15] which is developed based on three-dimensional elasticity theory and is defined by 20 nodes having three degrees of freedom at each node: translation in the node x, y and z directions.

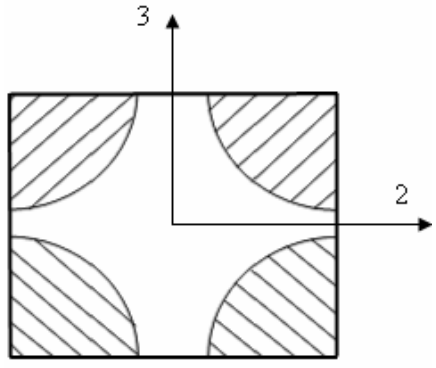

Fig. 2 — Isolated unit cell of square packed array

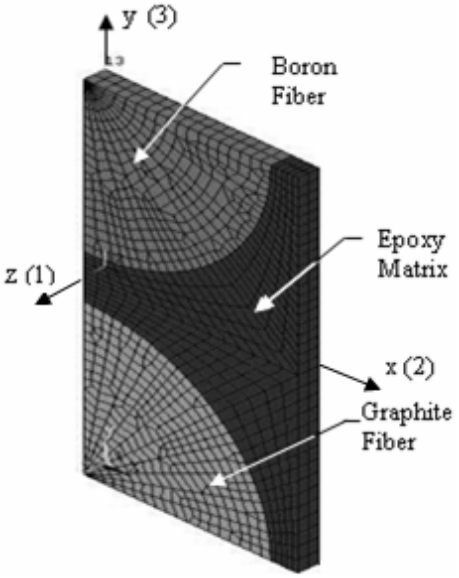

Fig. 3 — Finite element mesh on one-fourth portion of the unit cell

The properties of the constituent materials used for the present analysis are given in Table 1. Uniform tensile load of 1 MPa is applied on the area at X = 100 units.

Due to the symmetry of the problem, the following symmetric boundary conditions are used

at $x = 0$, $U_x = 0$
at $y = 0$, $U_y = 0$
at $z = 0$, $U_z = 0$

In addition the following multi point constraints are used.

The U_x of all the nodes on the line at x =100 is same
The U_y of all the nodes on the line at y =200 is same
The U_z of all the nodes on the line at z = 10 is same

Results and Discussion

The mechanical properties of the lamina are calculated using the following expressions. Young's modulus in in-plane transverse direction is determined using the formula

$$E_2 = \frac{\sigma^2}{\varepsilon_2}$$

where σ_2 is the stress in 2-direction (X) which is same as the pressure load applied in transverse direction. ε_2 is the strain in 2-direction (X) calculated from the displacement of the model in 2-direction obtained from finite element analysis.

Poisson's ratios are determined from the following equations

$$v_{21} = \frac{\varepsilon_1}{\varepsilon_2}; \quad v_{23} = \frac{\varepsilon_3}{\varepsilon_2}\,\frac{-\varepsilon_1}{\varepsilon_2}$$

where ε_1, ε_2 and ε_3 are the strains in longitudinal, in-plane transverse and out-of-plane transverse directions of the model respectively in the

Table 1 — Properties of constituents[7]

Material	E (GPa)	N	G (GPa)
Graphite fiber	E_1 =233	ν_{12} = 0.2	G_{12} = 8.96
	E_2 =23.1	ν_{13} = 0.2	G_{13} = 8.96
	E_3 =23.1	ν_{23} = 0.4	G_{23} = 8.27
Boron fiber	400	0.2	—
Epoxy matrix	4.62	0.36	—

corresponding directions and are calculated from the displacements obtained from the finite element analysis.

Sufficient numbers of convergence tests are made and the present finite element model is validated by comparing the Young's modulus of FP-Al lamina predicted with the value from the available literature[16] and found close agreement (Fig. 4). Figure 5 presents the mechanical properties predicted from the present analysis. Later the finite element models are used to evaluate the properties E_2, ν_{21}, ν_{23} and the stresses at the fiber matrix interface of a hybrid composite with boron and graphite fibers.

Variation of young's modulus (E_2) with respect to volume fraction

It is observed that there is a linear increment of the young's modulus with respect to volume fraction for all the three combinations up to $V_f = 45\%$. For V_f from 45% to 60% the young's modulus increases at a slow rate. For V_f between 60% and 75% it increases at faster rate for boron-epoxy and hybrid-epoxy composites. This is because the stiffness of the composite increases with increase in V_f. The young's modulus of boron-epoxy at all the volume fractions is observed to be maximum followed by hybrid-epoxy and graphite-epoxy, due to the less value of graphite fiber transverse modulus when compared with boron fiber modulus. (Fig. 5)

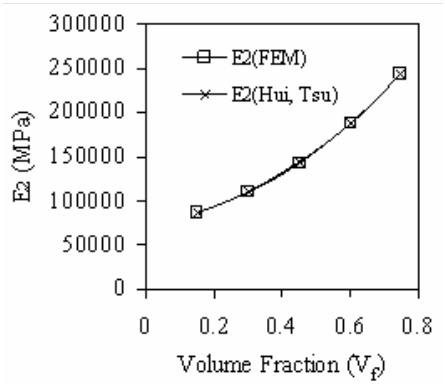

Fig. 4 — Variation of Young's modulus (E_2) with respect to volume fraction

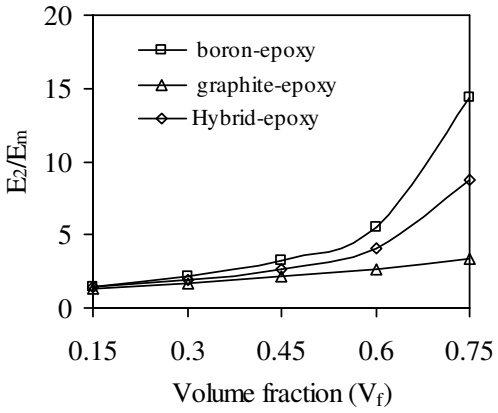

Fig. 5 — Variation of Young's Modulus (E_2) with respect to volume fraction

Variation of Poisson's ratio (ν_{21} and ν_{23}) with respect to volume fraction

The Poisson's ratio (ν_{21}) decreases from $V_f = 15\%$ to 45%, and later increases for boron-epoxy and hybrid-epoxy. For graphite-epoxy it shows a decreasing trend throughout. (Fig. 6)

The Poisson's ratio (ν_{23}) gradually decreases with the increase in volume fraction for all the three combinations (Fig. 7). The rate of decrease is more for boron-epoxy followed by hybrid-epoxy.

The following stresses are computed at the fiber-matrix interface (Fig. 8): (i) σ^f_n = normal stress in the fiber at the interface, (ii) σ^m_n = normal stress in the matrix at the interface, (iii) τ^f_{ns} = shear stress in the fiber at the interface, (iv) τ^m_{ns} = shear stress in the

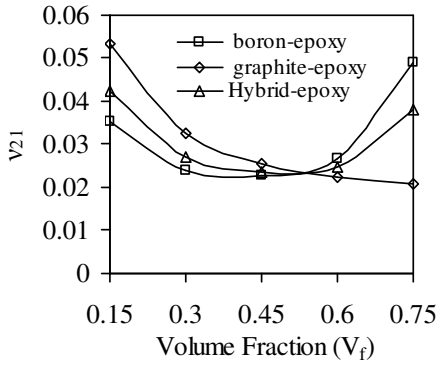

Fig. 6 — Variation of Poisson's ratio (ν_{21}) with respect to volume fraction

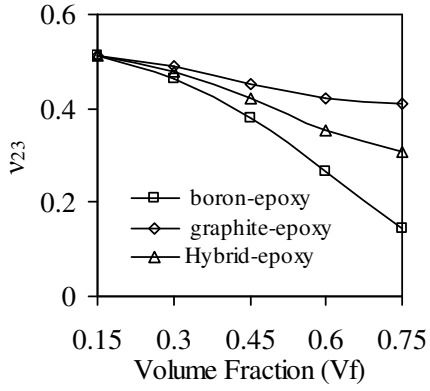

Fig. 7 — Variation of Poisson's Ratio (ν_{23}) with respect to volume fraction

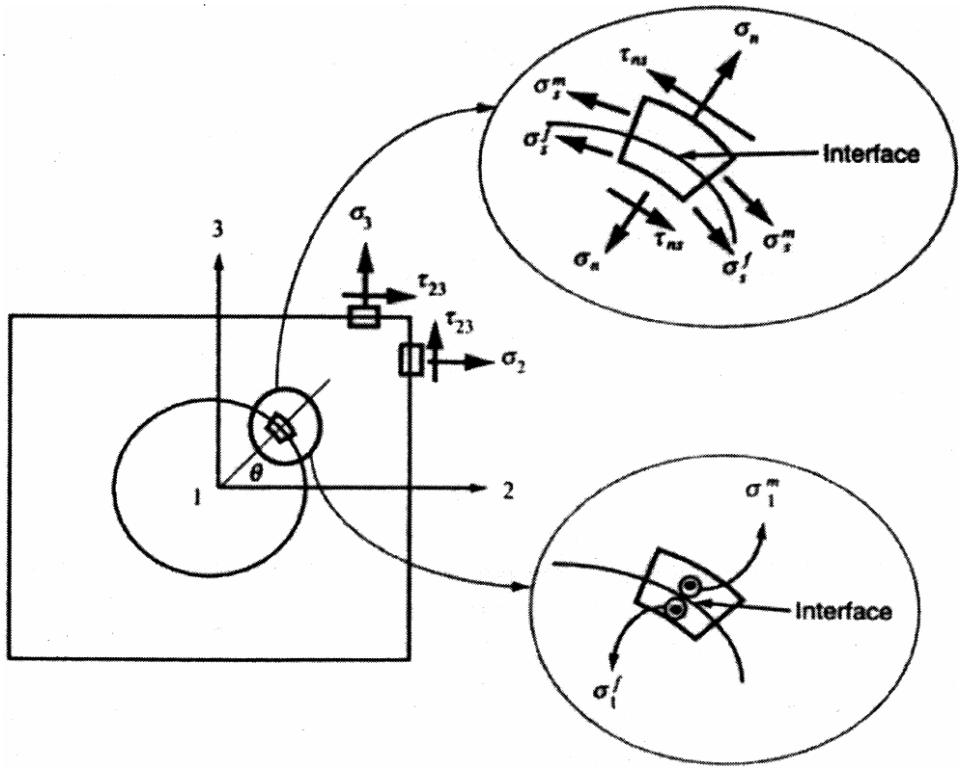

Fig. 8 — Unit cell showing the stresses at the interface and boundaries

matrix at the interface, (v) σ^f_c = circumferential stress in the fiber at the interface, (vi) σ^m_c = circumferential stress in the matrix at the interface, (vii) σ^f_1 = fiber directional stress in the fiber at the interface and (Viii) σ^m_1 = fiber directional stress in the matrix at the interface

Analysis of stresses at the interfaces

The results are normalised with the applied pressure, i.e., the uniform tensile load applied in the in-plane transverse direction (2-direction). Figures 9 and 10 show the variation of normal stress in fiber and matrix at the interface with respect to θ at the bottom and top interfaces respectively. Here θ is the angle measured simultaneously from bottom of the finite element model in counter clockwise direction for the bottom interface, and from top of the unit cell in clockwise direction for the top interface. For all the values of V_f the normal stress is tensile up to θ = 70° and is compressive between θ = 70° and θ = 90°. The magnitude of the stress is observed to be maximum at θ = 0° for all volume fractions. This is because at this location the applied force is normal to the interface. It is observed that the maximum stress decreases with increase in V_f. This is due to the reason that the resistance at the interface increases with increase in volume fraction.

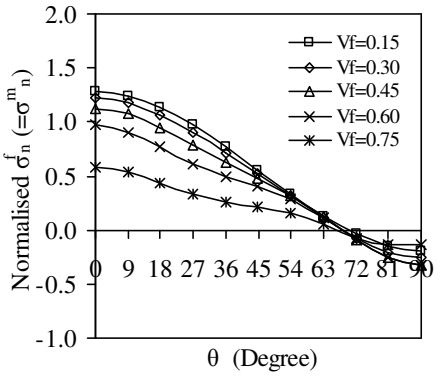

Fig. 9 — Variation of σ_n with respect to θ (bottom interface)

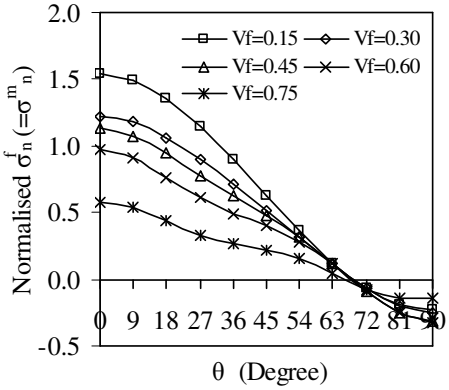

Fig. 10 — Variation of σ_n with respect to θ (top interface)

The variation of the shear stress at the bottom interface in the constituent materials with respect to θ is shown in Fig. 11. The magnitude of the shear stress is observed to be maximum at θ = 45° for volume fractions of 15% and 30%. For V_f = 45% and 75% stress is maximum at θ = 54°. For V_f = 60% this stress is maximum at θ = 63°. From the curves, it can be observed that the shearing action between the constituents is zero at the start and end values of θ and maximum at various locations for different values of V_f. The deviation of the maximum stress locations at higher volume fractions may be due to the effect of constraints imposed on boundaries of the FE model. It is also observed that the magnitude of maximum shear stress decreases with increase in V_f. This is due to the reason that the resistance at the interface increases with increase in volume fraction.

The variation of the interface shear stress at the top interface in both the constituent materials with respect to θ is shown in Fig. 12. The magnitude of the shear stress is observed to be maximum at θ = 45° for volume fractions of 15% and 30%. The shear stress is observed to maximum at θ = 27°,18° and 9° for volume fractions of 45%, 60% and 75% respectively. It is observed that the magnitude of the maximum shear stress decreases with increase in V_f. The reasons for the variation of stresses at top interface are similar to that discussed at the bottom interface. From Figs 11 and 12 it is noticed that the stresses are more at top interface. This is due to the high stiffness of boron fiber causing for higher reaction forces at the interface in shear.

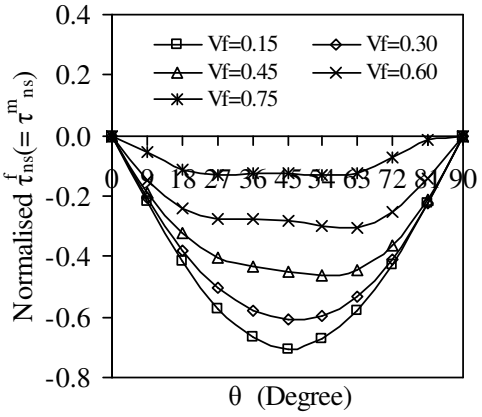

Fig. 11 — Variation of τ_{ns} with respect to θ (bottom interface)

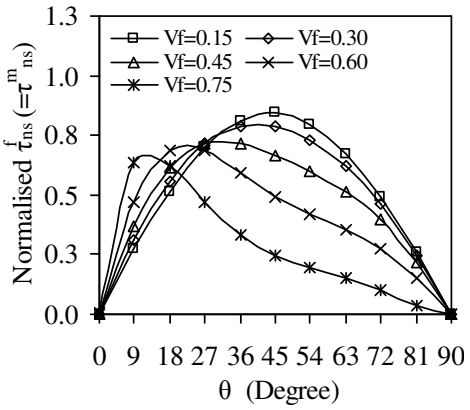

Fig. 12— Variation of τ_{ns} with respect to θ (top interface)

Figure 13 shows the variation of interface circumferential stress at the bottom interface in the fiber material with respect to θ. The stresses are observed to be tensile for V_f = 45%, 60% and 75%. For V_f = 15% the stress is observed to be compressive up to θ = 18° and is tensile in between 18° and 90°. For V_f = 30% the stress is observed to be compressive up to θ = 12° and is tensile in between 12° and 90°. The magnitude of the circumferential stress is observed to be maximum at θ = 90° for V_f from 15% to 60% . For V_f = 75% it is maximum at θ = 0°. The magnitude of the maximum circumferential stress decreases with increase in V_f. For lower volume fractions, the fiber surface at θ = 0° is subjected compression due to the action of matrix. As the angle θ increases, the matrix will try to pull the fiber surface and the stress will be tensile. As the volume fraction increases, the action of matrix decreases resulting in the reduction of magnitude of maximum stress and the stresses are positive for all the values of θ.

Figure 14 shows the variation of interface circumferential stress at the top interface in the fiber material with respect to θ. The stresses are observed to be compressive between θ = 0° to θ = 18° and then tensile in between θ = 18° to θ = 90° for V_f = 15%. For V_f =30% this stress is compressive up to θ = 12° and then tensile between θ = 12° to 90° . For V_f = 45%, 60% and 75% the stresses are observed to be tensile

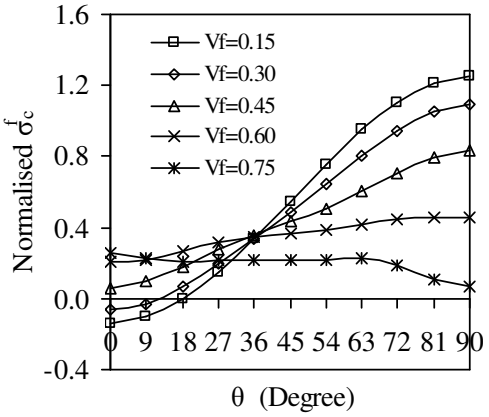

Fig. 13 — Variation of σ^f_c with respect to θ (bottom interface)

for all the values of θ. The magnitude of the circumferential stress is observed to be maximum at θ = 90° for volume fractions of 15%, 30% and 45%. For V_f = 60% the stress is maximum at θ = 36° and for V_f = 75% this stress is maximum at θ = 0° The magnitude of maximum circumferential stress decreases with increase in V_f up to 60% and for V_f = 75% it increases. At higher volume fractions, the tensile force applied in 2-direction causes contraction of the unit cell in 3-direction. This effect is more for matrix than in fiber. As a result the matrix tries to pull the fiber in 3-direction causing for positive stresses even to maximum at lower values of θ. The reasons for other variations are similar to that explained at bottom interface.

Figure 15 shows the variation of interface circumferential stress at bottom interface in the matrix material with respect to θ. The stresses are observed to be tensile for V_f = 15%, 30% and 45% for all the values of θ. For V_f = 60% the stress is observed to be tensile up to θ = 81° and is compressive in between 81° and 90°. For V_f = 75% the circumferential stress is observed to be tensile up to θ = 72° and is compressive in-between 72° to 90°. The magnitude of the circumferential stress is observed to be maximum at θ = 0° for all volume fractions. The magnitude of the maximum circumferential stress decreases with increase in V_f.

Figure 16 shows the variation of interface circumferential stress at top interface in the matrix material with respect to θ. The stresses are observed to be tensile for all V_f up to θ = 72° and it is compressive in between θ = 72° and 90°. The stresses are observed to be maximum at θ = 0° for all the volume fractions. The magnitude of the maximum circumferential stress increases with increase in V_f. As explained at Fig. 14, application of tensile force in 2-direction causes contraction of the unit cell in 3-direction. up to certain value of θ the circumferential stresses will setup due to the mismatch of the Poisson's ratios in the fiber and matrix materials. Since the mismatch is more between boron and epoxy than the graphite and epoxy, higher values of stresses are noticed at top interface than at bottom interface.

The variation of interfacial longitudinal normal stress at bottom interface in the fiber is shown in Fig. 17. The stresses are compressive in nature for all the values of θ and V_f. The magnitude of the stress is

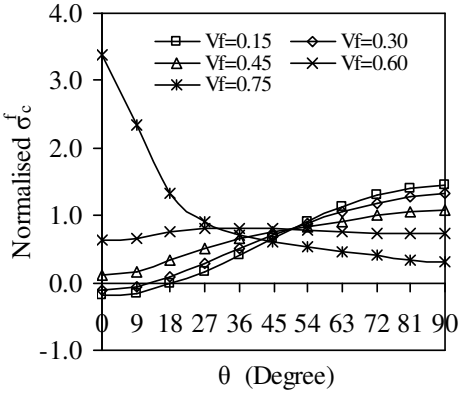

Fig. 14 — Variation of σ^f_c with respect to θ (top interface)

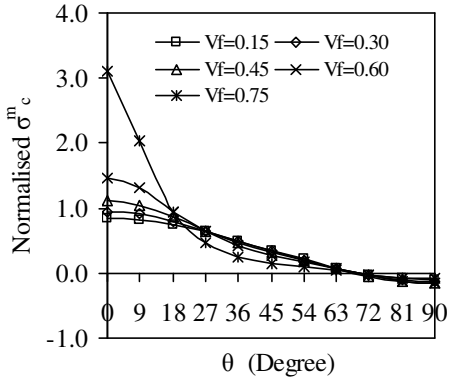

Fig. 16 — Variation of σ^m_c with respect to (top interface)

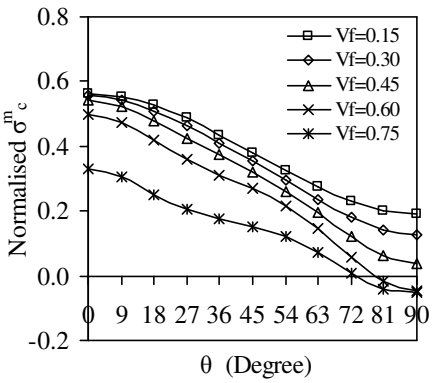

Fig. 15 — Variation of σ^m_c with respect to (bottom interface)

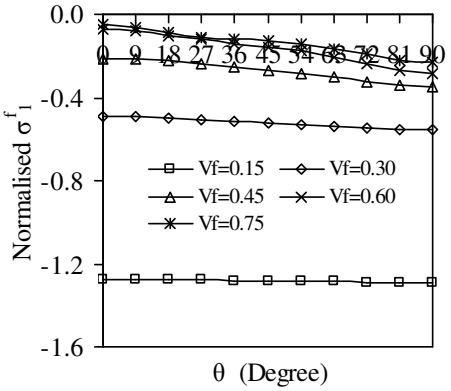

Fig. 17 — Variation of σ^f_1 with respect to θ (bottom interface)

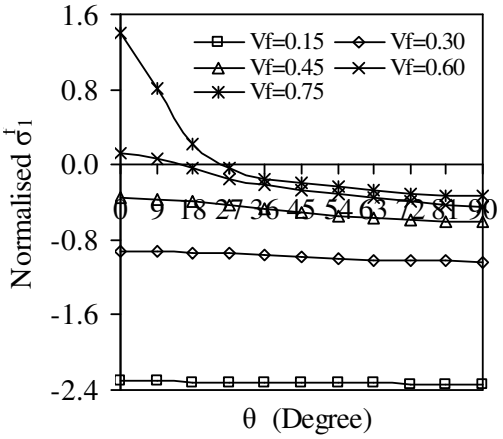

Fig. 18 — Variation of σ^f_1 with respect to θ (top interface)

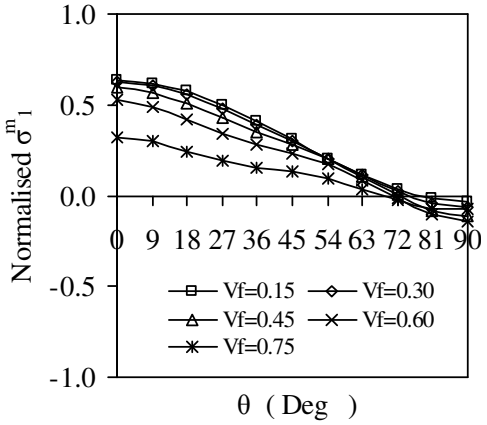

Fig. 19 — Variation of σ^m_1 with respect to θ (bottom interface)

observed to be maximum at θ = 90° for all volume fractions. It is observed that the maximum stress decreases with increase in volume fraction.

The variation of interfacial longitudinal normal stress at top interface in the fiber is shown in Fig. 18. The stresses are compressive for V_f =15%, 30%, 45% for all values of θ. For V_f = 60% this stress is tensile up to θ = 18° and is compressive in between θ = 18° to 90°. For V_f =75%, this stress is observed to be tensile up to θ = 27° and is compressive in between θ = 27° to θ = 90°. The magnitude of stress is observed to be maximum at θ = 90° for V_f =15%, 30%, 45% and 60%. For V_f = 75% this stress is maximum at θ = 0°. The magnitude of the interfacial longitudinal normal stress decreases with increase in V_f except for V_f = 75%.

The variation of interfacial longitudinal normal stress at bottom interface in the matrix is shown in Fig. 19. The stresses are tensile in nature for all the values of V_f up to θ = 72° and is compressive between θ = 72° to 90^0. The magnitude of the stress is observed to be maximum at θ = 0°. It is observed that the maximum stress decreases with increase in V_f.

The variation of interfacial longitudinal normal stress at top interface in the matrix is shown in Fig. 20. The stresses are tensile in nature for all the values of V_f up to θ = 72° and is compressive in between θ = 72° to 90^0. The stresses are observed to be maximum at θ = 0° for all the volume fractions. The magnitude of the interfacial longitudinal normal stress increases with the increase in volume fraction.

The main reason for the longitudinal stresses at the interfaces is the mismatch of the Poisson's ratios in the constituents (Figs 16-20). The matrix tries to compress the fiber causing for compressive stresses in fiber and tensile stresses in matrix at the interface. As

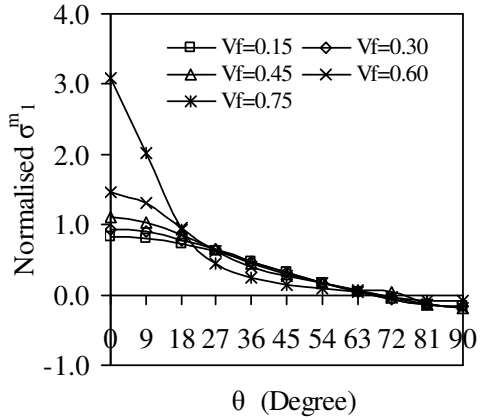

Fig. 20 — Variation of σ^m_1 with respect to θ (top interface)

the volume fraction increases, the action of the matrix decreases resulting in the reduction of the stresses. Since the mismatch is more at the top interface, the stresses at this interface are more than that at the bottom interface. Any deviations other than above are due to the effect of constraints imposed on the boundaries of the unit cell.

Conclusions

The micromechanical behaviour of hybrid FRP lamina has been studied using finite element method. The Young's modulus E_2 and Poisson's ratios ν_{21} and ν_{23} are predicted for different fiber volume fractions. The stresses at the fiber-matrix interface are also computed. The following conclusions are drawn.

(i) The Young's modulus is found to be increasing with V_f indicating that the stiffness of the composite increases with V_f.

(ii) The Poisson's ratios (ν_{23}) decreases with the increase in volume fraction for all the three combinations.

(iii) The magnitude of the normal stresses at the fiber matrix interface are maximum at $\theta = 0°$ as the direction of the load is normal to the surface at this location. This may result in the separation of fiber and matrix leading to debonding. (Figs 9 and 10).

(iv) The magnitude of the shear stress is observed to be maximum at $\theta = 45°$ in many cases indicating that the interfacial damage may occur at these locations. (Figs 11 and 12).

(v) The magnitude of circumferential stresses in the fiber material is observed to be maximum at $\theta = 90°$ for lower volume fractions and at $\theta = 0°$ for higher volume fractions. These are due to the reasons of load in 2-direction and mismatch in Poisson's ratios respectively. This may result in the failure of the fiber at these locations. (Figs 13 and 14).

(vi) The circumferential stress of matrix material is found to be maximum at $\theta = 0°$. This is due to the mismatch in Poisson's ratios. This indicates that the failure of the matrix may originate at this location. (Figs 15 and 16).

The present analysis is useful to identify the hybrid effect in selecting the materials for reasonable properties. It is also useful to identify the locations where the failure of the interface takes place and that can be modeled as an imperfection for obtaining the properties of the composite with fiber-matrix interface debond.

References

1 Chen C H & Cheng S, *Trans ASME J Appl Mech*, 37(1970)186-189.
2 Hashin Z & Rosen B W, *Trans ASME J Appl Mech*, 31 (1964) 223-232.
3 Hashin Z, *J Mech Phys Solids*, 13 (1965) 119-134.
4 Whitney J M, *J Compos Mater*, 1(1967) 88-193.
5 Takashi Ishiwaka, Koyama K & Kobayashi S, *J Compos Mater*, 11 (1977) 332-344.
6 Hashin Z, *Trans ASME J Appl Mech*, 50 (1983) 481-505.
7 Hyer M W, *Stress Analysis Fiber-Reinforced Composite Materials*, (Mc. Graw-Hill International edition), 1998.
8 Mohana Rao K, *Work Shop on Introduction to Fiber-Reinforced Composite*, NSTL, 1986.
9 Morais A B, *Compos Sci Technol*, 60 (2000) 997-1002.
10 Anifantis N K, *Compos Sci Technol*, 60 (2000) 1241-1248.
11 Sun C T & Vaidya R S, *Compos Sci Technol*, 56 (1996)171-179.
12 Li S, *Composites: Pt A*, 32 (2000) 815-826.
13 Yiping Qiu & Peter Schwartz, *Compos Sci Technol*, 47 (1993) 289-301.
14 Mishra & Mohanty, *Compos Sci Technol*, 63 (2003) 1377-1385.
15 *ANSYS Reference Manuals*, 2006.
16 Hui-Zushan & Tsu- Wei Chout, *Compos Sci Technol*, 53 (1995) 383